Canadian Mineralogist
Vol. 22, pp. 605-619 (1984)

METAMORPHIC PETROLOGY OF THE JACKSON COUNTY IRON FORMATION, WISCONSIN

KAREN L. KIMBALL*
Department of Geology and Geophysics, University of Wisconsin, Madison, Wisconsin 53706, U.S.A.

FRANK S. SPEAR
Department of Earth, Atmospheric and Planetary Sciences, Massachusetts Institute of Technology, Cambridge, Massachusetts 02139, U.S.A.

ABSTRACT

The Jackson County Iron Formation, central Wisconsin, is a metamorphosed Precambrian banded iron-formation of probable Archean age. Two metamorphic events are recorded in the rocks: the first with a probable peak P and T of 3.5 kbar and 550°C, and the second at a slightly lower T. Two assemblages predominate: 1) actinolite + cummingtonite + quartz + magnetite ± riebeckite ± biotite ± hematite ± pyrite and 2) hornblende + cummingtonite + garnet + quartz + magnetite ± ilmenite ± pyrite ± carbonate ± plagioclase ± biotite. Variations in the $Fe^{2+}/(Fe^{2+}+Mg)$ values of coexisting amphiboles within a sample ($X_{Fe,cum} \cong X_{Fe,hbl} > X_{Fe,act}$) reflect the crystallographic site-preferences of the major cations. Mg^{2+} and Al^{3+} are partitioned preferentially into *M*2 and Fe^{2+} and Ca^{2+} into *M*4. Variations in the compositions of the amphiboles between beds are the results of premetamorphic differences in bulk composition and gradients in the chemical potentials of O_2 and H_2O. An increase in $\mu(O_2)$ at constant $\mu(H_2O)$, P and T decreases the grunerite component in a given amphibole. An increase in $\mu(H_2O)$ at constant $\mu(O_2)$, P and T increases the grunerite component. Estimated gradients in $\Delta\mu(O_2)$ and $\Delta\mu(H_2O)$ range from 1 to 65 cal/m and 1 to 76 cal/m, respectively. The unusual occurrence of riebeckite as inclusions in cummingtonite is interpreted as incomplete alteration of an original riebeckite-bearing bed in the iron formation and suggests that the protolith may have formed in a closed basin. Riebeckite along cracks in cummingtonite is interpreted as being a feature of late-stage alteration.

Keywords: iron formation, amphibole, solution model, riebeckite, chemical potential gradients, Wisconsin.

SOMMAIRE

La formation de fer rubanée du comté de Jackson, au Wisconsin, est probablement d'âge archéen. Deux événements métamorphiques auraient affecté ces roches, le premier à 3.5 kbar et 550°C, le second à une température légèrement inférieure à ceci. Deux assemblages sont répandus: 1) actinote + cummingtonite + quartz + magnétite ± riebeckite ± biotite ± hématite ± pyrite et 2) hornblende + cummingtonite + grenat + quartz + magnétite ± ilménite ± pyrite ± carbonate ± plagioclase ± biotite. Les variations dans le rapport $Fe^{2+}/(Fe^{2+}+Mg)$ des amphiboles coexistant dans un même échantillon ($X_{Fe,cum} \cong X_{Fe,hbl} > X_{Fe,act}$) résultent de la préférence des cations majeurs dans les diverses positions cristallographiques: Mg^{2+} et Al^{3+} préfèrent *M*2, et Fe^{2+} et Ca^{2+}, *M*4. Les variations dans la composition des amphiboles entre couches résultent des différences prémétamorphiques dans le chimisme des roches et des gradients dans le potentiel chimique de O_2 et de H_2O. Une augmentation en $\mu(O_2)$ à $\mu(H_2O)$, T et P constants diminue la concentration du pôle grunerite dans une amphibole. Une augmentation en $\mu(H_2O)$ à $\mu(O_2)$, P et T constants augmente la teneur en grunerite. Les gradients $\Delta\mu(O_2)$ et $\Delta\mu(H_2O)$ ont une valeur entre 1 et 65 cal/m et 1 et 76 cal/m, respectivement. La présence inattendue de la riebeckite incluse dans la cummingtonite serait due à l'altération incomplète d'un lit originellement riebeckitique dans la formation de fer, et fait penser que cette roche pourrait s'être formée dans un bassin fermé. La riebeckite qui tapisse les fissures dans la cummingtonite serait due à une altération tardive.

(Traduit par la Rédaction)

Mots-clés: formation de fer, amphibole, modèle de solution, riebeckite, gradient en potentiel chimique, Wisconsin.

INTRODUCTION

Amphiboles occur in a wide variety of igneous and metamorphic environments. This widespread occurrence makes them extremely important as potential petrogenetic indicators. Phase relations among metamorphic amphiboles were used in deriving the metamorphic facies concept (*e.g.*, Eskola 1915) and as an indication of metamorphic environment (Laird & Albee 1981). This study is an attempt to further clarify the phase relations of these minerals by investigating the effects of bulk composition, cation site-preference, $\mu(O_2)$ and $\mu(H_2O)$ on amphiboles found in the Jackson County Iron Formation, Wisconsin.

GEOLOGICAL SETTING

The orebody at the Jackson County iron mine is a late Archean, Algoma-type iron formation (2800 Ma, R. Maas, pers. comm., Jones 1978). It crops

*Present address: Department of Earth, Atmospheric and Planetary Sciences, Massachusetts Institute of Technology, Cambridge, Massachussetts 02139, U.S.A.

TABLE 1. MINERAL ASSEMBLAGES IN THE JACKSON COUNTY IRON FORMATION

Sample #	ACT	CUM	RBK	HBL	GRT	BT	QTZ	MAG	HEM	ILM	PY	CB
1692/3	X	X	X			X	X	X				
1692/12	X	X					X	X				
1733/1	X	X					X	X				
1733/2	X	X					X	X				
23-2-479	X	X					X	X				
386	X	X					X	X				X
15-5-289A	X	X					X	X				
15-5-289B		X		X	X	X	X	X				
1733/6		X		X	X		X		X	X		
1692/5		X		X	X		X		X	X		
1733/4		X		X	X		X		X	X		
1692/1		X		X	X		X		X	X		
469	X	X		X		X	X	X				
9-3-164	X			X	X	X	X	X				
1692/11	X						X	X	X			
1733/3	X	X		X	X	X	X	X			X	

ACT actinolite-ferroactinolite, CUM cummingtonite-grunerite, RBK riebeckite, HBL horublende-tachermakitic hornblende, GRT garnet, BT biotite, QTZ quartz, MAG magnetite, HEM hematite, ILM ilmenite, PY pyrite, CB carbonate

out in a lens 915 metres long and 150 metres thick, is enclosed by biotite-bearing pelitic schist, and is isoclinally folded around a talc schist core (Fig. 1). The iron formation exhibits distinct compositional banding, with alternating quartz-rich and magnetite-rich layers from less than 1 mm to more than 20 cm thick.

Textural and phase relations in the iron formation and surrounding pelitic schists suggest two metamorphic events (Jones 1978). The first event occurred between 500° and 600°C and at a pressure near 3 kbar, based on the reaction staurolite + chlorite = andalusite + biotite in the pelitic schist. This episode was accompanied by deformation and can probably be correlated with the Penokean orogeny in the area (>1840, <2800 Ma: R. Maas, pers. comm.). A second metamorphic event is characterized by the formation of kyanite, a second generation of staurolite replacing kyanite and andalusite, and hornblende replacing garnet. This event occurred at the same pressure, but at a slightly lower temperature (450–500°C) than the first event.

In the iron formation, the first metamorphic event is manifested by the development of amphiboles (cummingtonite ± actinolite ± hornblende), garnet, oxides and, in one sample, clinopyroxene. The second event resulted in replacement of garnet by second-generation hornblende (in some instances

TABLE 2. COMPOSITIONS* OF COEXISTING AMPHIBOLES FROM THE JACKSON COUNTY IRON FORMATION

Sample #	1692/3			1692/12		1733/1		1733/2		15-5-289		386	
Amphibole††	ACT	CUM	RBK	ACT	CUM	ACT	CUM	ACT	CUM	ACT	CUM	ACT	CUM
						WT. % OXIDES							
SiO_2	55.48	54.00	51.29	49.89	49.11	49.90	49.34	50.02	49.66	49.94	51.61	48.75	49.87
Al_2O_3	0.83	0.23	0.21	0.75	0.42	0.87	0.34	1.70	0.26	3.51	0.39	2.28	0.36
TiO_2	0.0	0.0	0.05	1.04	0.0	0.0	0.0	0.0	0.0	0.17	0.09	0.07	0.07
MgO	17.52	17.00	2.53	4.59	4.86	4.39	3.84	5.51	5.11	9.41	9.95	4.81	4.52
FeO†	12.46	26.29	34.44	30.62	43.48	32.34	45.41	30.92	43.66	23.57	34.24	31.54	41.64
MnO	0.0	0.0	0.14	0.07	0.0	0.0	0.0	0.0	0.0	0.18	0.58	0.10	0.10
CaO	11.98	1.11	0.45	10.99	1.24	10.87	0.64	11.28	0.61	10.87	1.13	10.77	1.04
Na_2O	0.0	0.0	6.08	0.11	0.0	0.0	0.0	0.0	0.0	0.50	0.04	0.12	0.14
K_2O	0.0	0.0	0.09	0.08	0.0	0.0	0.0	0.0	0.0	0.13	0.02	0.14	0.03
Total	98.27	98.63	95.28	98.14	99.11	98.37	99.57	99.43	99.30	98.28	98.05	98.58	97.77
						CATIONS PER 23 OXYGENS							
Si	7.864	7.915	7.981	7.870	7.850	7.830	7.899	7.692	7.901	7.510	7.953	7.627	7.999
Al^{IV}	0.136	0.040	0.019	0.130	0.079	0.161	0.064	0.308	0.049	0.490	0.047	0.373	0.001
Al^{VI}	0.003	0.0	0.020	0.010	0.0	0.0	0.0	0.0	0.0	0.133	0.023	0.048	0.067
Ti	0.0	0.0	0.006	0.005	0.0	0.0	0.0	0.0	0.0	0.019	0.010	0.008	0.008
Fe^{3+}	0.134	0.0	1.737	0.061	0.0	0.0	0.0	0.119	0.0	0.148	0.0	0.0	0.0
Mg	3.701	3.714	0.588	1.079	1.158	1.027	0.916	1.263	1.212	2.109	2.285	1.121	1.080
Fe^{2+}	1.343	3.223	2.754	3.978	5.812	4.244	6.080	3.857	5.809	2.817	4.412	4.127	5.586
Mn	0.0	0.0	0.018	0.009	0.0	0.0	0.0	0.0	0.0	0.023	0.076	0.013	0.014
Ca	1.819	0.174	0.075	1.858	0.212	1.828	0.110	1.863	0.104	1.752	0.187	1.805	0.179
Na(M4)	0.0	0.0	1.802	0.0	0.0	0.0	0.0	0.0	0.0	0.0	0.007	0.0	0.036
Na(A)	0.0	0.0	0.036	0.034	0.0	0.0	0.0	0.0	0.0	0.146	0.005	0.036	0.0
K	0.0	0.0	0.018	0.016	0.0	0.0	0.0	0.0	0.0	0.025	0.004	0.028	0.028
Sum A	0.0	0.0	0.054	0.050	0.0	0.0	0.0	0.0	0.0	0.171	0.009	0.064	0.028
$Fe^{3+}/(Fe^{3+}+Fe^{2+})$	0.090	0.000	0.387	0.015	0.0	0.0	0.0	0.030	0.006	0.050	0.0	0.0	0.0
$Fe^{2+}/(Fe^{2+}+Mg)$	0.266	0.465	0.824	0.787	0.834	0.805	0.869	0.753	0.827	0.572	0.659	0.838	0.786

† Total Fe as FeO

†† Abbreviations as in Table 1

* determined by electron microprobe analyses at 15 Kev. Riebeckite analyses made on the MIT MAC microprobe using synthetic pyroxene ($Di_{65}Jd_{35}$), Amelia albite, cosserite, rhodonite and orthoclase glass as standards. All other

leading to complete pseudomorphs), biotite or chlorite. The phase relations among the original coexisting amphiboles appear to have been largely undisturbed by the second event.

Mineralogy and Petrology of the Iron Formation

There are two predominant mineral assemblages in the iron formation: (1) actinolite + cummingtonite + quartz + magnetite ± riebeckite ± biotite ± hematite ± pyrite and 2) hornblende + cummingtonite + garnet + quartz + magnetite ± ilmenite ± pyrite ± carbonate ± plagioclase ± biotite. Representative assemblages of minerals are given in Table 1. These assemblages occur in different layers of the iron formation and reflect local variations in bulk composition; specifically, garnet and hornblende (assemblage 2) occur in the aluminous layers.

The talc schist core of the iron formation (Fig. 1) consists of pure talc or talc + cummingtonite + anthophyllite. Locally, the assemblages talc + magnetite, talc + biotite and talc + chlorite + andalusite + anthophyllite ± biotite ± garnet are present. There is a tendency for the iron formation to become more Al- and Mg-rich toward the talc schist, and the borders of the talc schist are more aluminous than the core.

Representative compositions of coexisting amphiboles from the iron formation are presented in Table 2. They differ in assemblages 1 and 2 and, for each assemblage, from layer to layer in the iron formation. In the next section we will discuss the composition of the amphiboles and some of the pertinent controls.

Cummingtonite - actinolite

The Fe-Mg amphiboles of the cummingtonite-grunerite series found in the Jackson County Iron Formation (JCIF) span the compositional range from $Fe^{2+}/(Fe^{2+} + Mg) = 0.39$ to 0.87, and in actinolite-ferroactinolite, $Fe^{2+}/(Fe^{2+} + Mg)$ ranges

Sample #	1733/6		1692/5		1733/4		1692/1		469		9-3-164			1692/11
Amphibole*	HBL	CUM	HBL	CUM	HBL	CUM	HBL	CUM	ACT	HBL	CUM	ACT	HBL	CUM
							WT. % OXIDES							
SiO_2	41.55	50.66	41.07	50.43	39.53	50.10	42.00	51.83	49.32	45.16	49.98	51.81	41.71	54.73
Al_2O_3	14.04	0.66	14.48	0.99	14.33	0.47	11.00	0.46	2.44	5.99	0.42	2.06	10.96	0.43
TiO_2	0.35	0.0	0.25	0.0	0.0	0.0	0.0	0.0	0.17	0.37	0.08	0.05	0.18	0.0
MgO	3.94	7.64	3.85	9.49	2.86	6.51	5.90	10.67	6.57	5.05	6.40	12.72	6.36	20.00
FeO	27.94	40.06	26.82	37.12	28.79	41.17	26.33	35.56	27.71	28.67	39.62	18.23	24.76	22.49
Mno	0.00	0.0	0.0	0.0	0.0	0.0	0.0	0.0	0.15	0.21	0.51	0.27	0.23	0.0
CaO	10.42	0.34	10.78	0.62	10.48	0.36	10.04	0.62	10.95	10.97	1.04	11.89	11.37	0.44
Na_2O	0.87	0.0	1.08	0.0	1.14	0.0	1.08	0.0	0.27	0.60	0.07	0.41	1.18	0.0
K_2O	0.33	0.0	0.31	0.0	0.59	0.0	0.64	0.0	0.17	0.72	0.05	0.19	1.04	0.0
Total	99.44	99.36	98.64	98.65	97.72	98.61	96.99	99.14	97.75	97.74	98.17	97.63	97.79	98.09
							CATIONS PER 23 OXYGENS							
Si	6.310	7.887	6.283	7.813	6.317	7.917	6.540	7.906	7.615	7.061	7.920	7.661	6.428	7.902
Al^{IV}	1.690	0.113	1.717	0.181	1.683	0.083	1.460	0.083	0.385	0.939	0.078	0.339	1.572	0.073
Al^{VI}	0.824	0.008	0.895	0.0	1.031	0.005	0.559	0.0	0.059	0.165	0.0	0.020	0.419	0.0
Ti	0.040	0.0	0.029	0.0	0.0	0.0	0.0	0.0	0.020	0.044	0.010	0.006	0.021	0.0
Fe^{3+}	0.466	0.0	0.384	0.0	0.085	0.0	0.381	0.0	0.172	0.361	0.0	0.155	0.554	0.0
Mg	0.892	1.773	0.878	2.191	0.678	1.533	1.369	2.426	1.512	1.177	1.511	2.803	1.461	4.303
Fe^{2+}	3.083	5.216	3.048	4.809	3.352	5.441	3.048	4.537	3.406	3.388	5.251	2.099	2.638	2.716
Mn	0.0	0.0	0.0	0.0	0.0	0.0	0.0	0.0	0.020	0.028	0.068	0.034	0.030	0.0
Ca	1.696	0.057	1.767	0.103	1.854	0.061	1.675	0.101	1.812	1.838	0.177	1.884	1.878	0.068
Na(M4)	0.0	0.0	0.0	0.0	0.0	0.0	0.0	0.0	0.0	0.0	0.0	0.0	0.0	0.0
Na(A)	0.256	0.0	0.320	0.0	0.440	0.0	0.326	0.0	0.081	0.182	0.022	0.118	0.353	0.0
K	0.064	0.0	0.061	0.0	0.127	0.0	0.127	0.0	0.033	0.144	0.0	0.036	0.204	0.0
Sum A	0.320	0.0	0.381	0.0	0.567	0.0	0.460	0.0	0.114	0.326	0.022	0.154	0.557	0.0
$Fe^{3+}/(Fe^{3+}+Fe^{2+})$	0.130	0.0	0.112	0.0	0.025	0.0	0.111	0.0	0.048	0.096	0.0	0.069	0.173	0.0
$Fe^{2+}/(Fe^{2+}+Mg)$	0.776	0.746	0.776	0.687	0.832	0.687	0.690	0.652	0.693	0.742	0.777	0.428	0.644	0.387

analyses obtained at the University of Chicago on an ARL microprobe using Kakanui hornblende as the standard. Mössbauer analyses of several amphiboles (Kimball, 1981) indicate that very little Fe^{3+} is present in actinolite or cummingtonite (<10% Fe total). Minimum Fe^{3+} based on stoichiometric considerations (Spear and Kimball 1983) is reported.

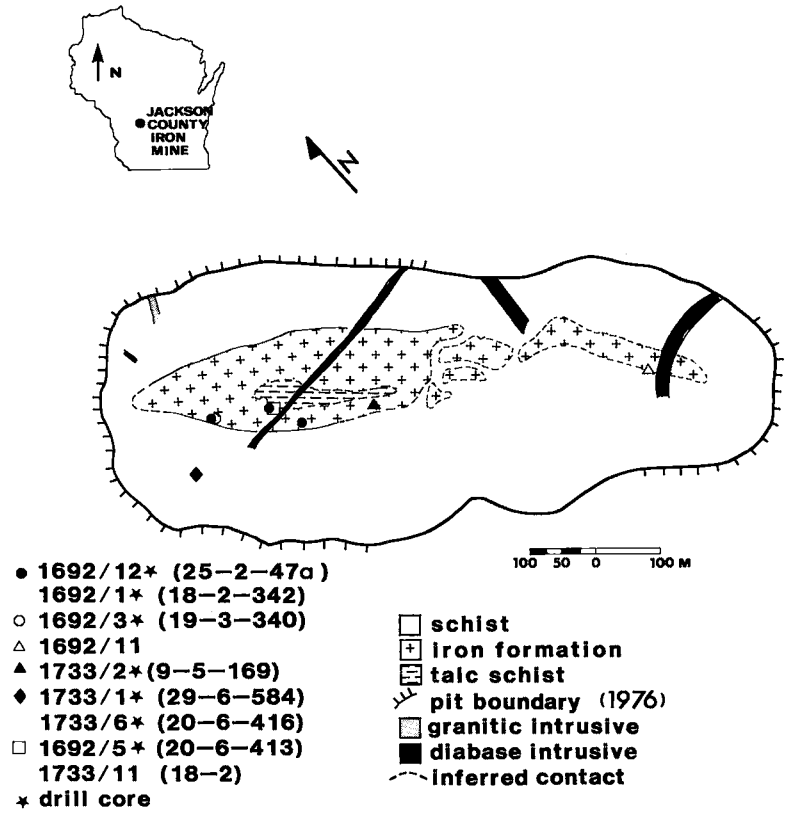

FIG. 1. Schematic geological map of the Jackson County Iron Mine. The outline of the pit dates from 1976, when the drilling was done. Sample locations are plotted and geological contacts drawn as they appeared in 1976.

from 0.27 to 0.84. As a rule, the most Mg-rich amphiboles are found only in magnetite-rich layers of the iron formation, and the most Fe-rich amphiboles are found in the magnetite-poor layers. Comparison of amphibole compositions in Table 2 shows that in general, the more Mg-rich amphiboles, cummingtonite or actinolite, contain more SiO_2 and less Al_2O_3 than their Fe-rich counterparts, grunerite and ferroactinolite.

Figure 2a shows pairs of coexisting amphiboles on the amphibole quadrilateral diagram. Note that the calcic amphibole has a significantly lower $Fe^{2+}/(Fe^{2+} + Mg)$ value than the Fe–Mg amphibole (see also Table 2).

Hornblende

Hornblende in the Jackson County Iron Formation ranges in composition from ferro-hornblende to ferro-tschermakite (Leake 1978) and has two distinct modes of occurrence. The most abundant is hornblende associated with garnet–cummingtonite–quartz–ilmenite. This hornblende clearly replaces garnet. In some cases, the garnet is rimmed by hornblende, whereas in others hornblende rims the garnet and also follows cracks within it, and in some cases garnet is completely replaced by hornblende, leaving only the pseudomorph. In this association, the hornblende is interpreted as being secondary, a product of the second metamorphic event. The other occurrence is hornblende with actinolite or cummingtonite, not directly associated with garnet. In this occurrence no reaction textures are apparent, and hornblende is interpreted as being a product of the first metamorphic event. Coexisting hornblende–cummingtonite pairs are plotted on an ACF diagram (Fig. 2b). Note that the hornblende coexisting with actinolite (sample 469, Fig. 2b) has the lowest Al_2O_3 content.

In the hornblende–cummingtonite pairs, hornblende and cummingtonite have similar $Fe^{2+}/(Fe^{2+} + Mg)$ (Table 2). Qualitative energy-dispersion spectra indicate ½ to 1% Cl in hornblende from samples 469, 9-3-164 and 1692/1.

Riebeckite

Riebeckite occurs in a variety of textures, and its origin is still uncertain. Photomicrographs of different textural relations are shown in Figure 3. The most significant occurrences are: 1) riebeckite 'core' in cummingtonite (Fig. 3a) and 2) riebeckite in fractures (Figs. 3b, 3c and 3d). The composition of this riebeckite (Table 2) is similar to that of the massive riebeckite found in Australian iron formations (Miyano & Klein 1983). To our knowledge, the three-phase assemblage cummingtonite–actinolite–riebeckite had not been reported previously.

The riebeckite textures shown indicate at least two different origins for the riebeckite. The core relationship (Fig. 3a) suggests that the riebeckite was a precursor to cummingtonite in the metamorphism of the iron formation. In the fracture occurrence (Figs. 3b, 3c and 3d), riebeckite is always located along cracks in cummingtonite; commonly these cracks intersect magnetite inclusions within cummingtonite (*cf.* Figs. 3c and 3d). This suggests that this riebeckite formed by late-stage alteration of cummingtonite and magnetite. Subsequent modification of this alteration by exsolution of actinolite from cummingtonite has generated the curious "step" pattern (*e.g.*, Fig. 3b). Backscattered electron imaging of this texture (Fig. 3c) reveals that the actinolite lamellae separate the cummingtonite from the riebeckite. An alternative hypothesis, that the riebeckite is not a late-stage alteration but an early phase subsequently modified by exsolution processes, cannot be ruled out.

Two other alkali amphibole–cummingtonite pairs have been described, arfvedsonite–cummingtonite in New Caledonia (Black 1973) and riebeckite–cummingtonite in Labrador (Klein 1966, 1968). These two pairs are plotted with the three-amphibole assemblage from the Jackson County Iron Formation (Fig. 4). The association riebeckite-actinolite is present in the Carter Creek iron deposit, Ruby Mountains, Montana (Immega & Klein 1976), and those pairs are also plotted in Figure 4. Many other sodic-calcic and sodic-Fe–Mg amphibole pairs have

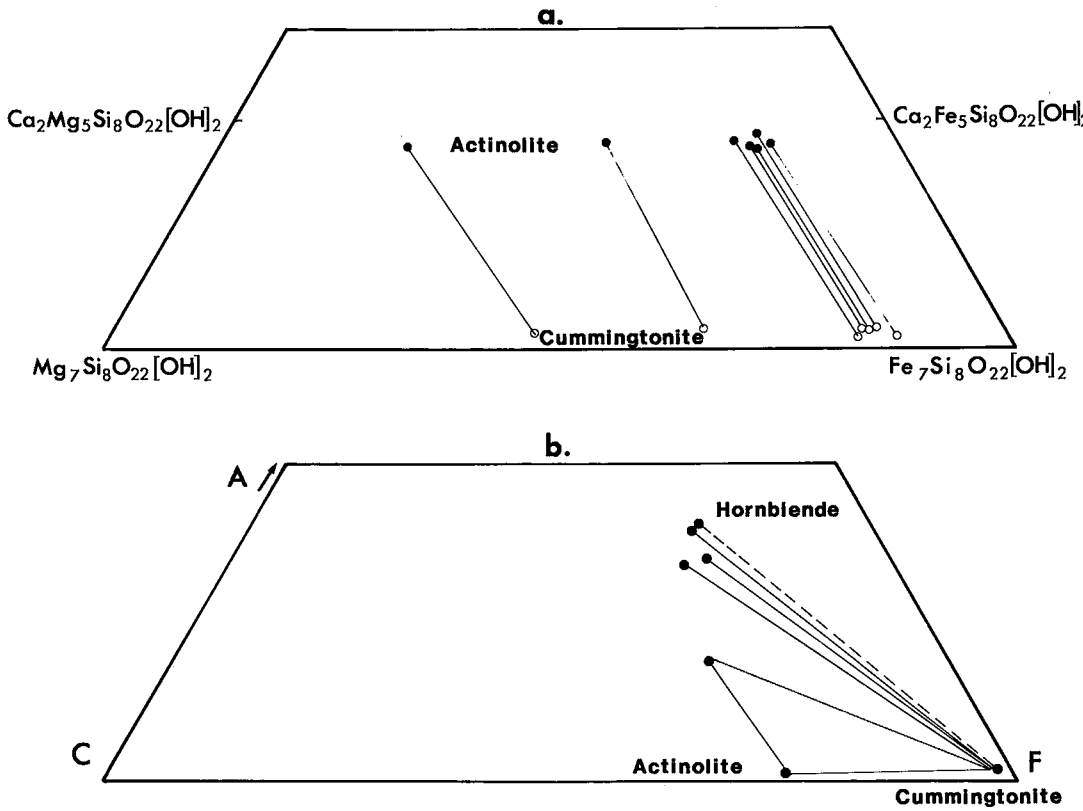

FIG. 2. a) Amphibole quadrilateral. Actinolite–cummingtonite pairs from the Jackson County Iron Formation are connected by tielines. b) ACF plot of hornblende–cummingtonite pairs. One three-phase assemblage hornblende – cummingtonite – actinolite is also plotted.

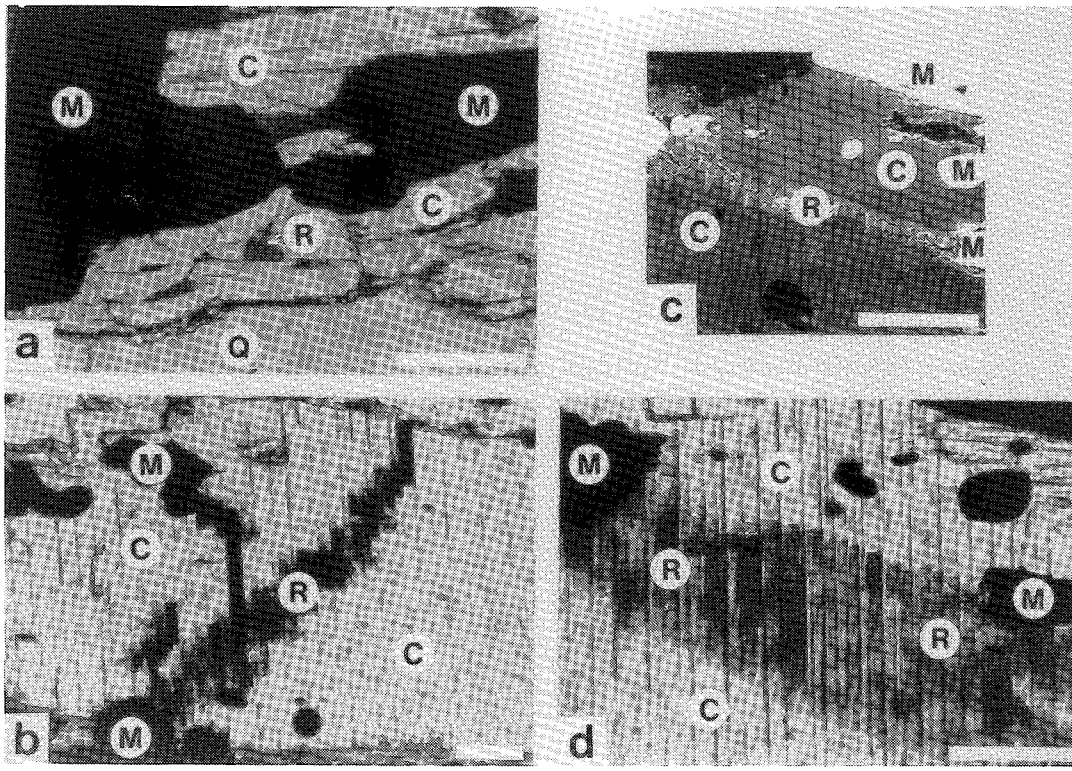

FIG. 3. Photomicrographs of riebeckite. White bars represent 50 μm. R riebeckite, C cummingtonite, A actinolite, M magnetite, Q quartz. a) Riebeckite core in cummingtonite. b) Riebeckite in fractures in cummingtonite. c) Backscattered electron photomicrograph of riebeckite along a crack between two magnetite grains; same area as shown in Fig. 3d. d) Riebeckite along fracture in cummingtonite separated by exsolution lamellae of actinolite. In this last photomicrograph, riebeckite appears as a wide band, but is actually a thin layer ($\sim$10 μm thick) that slopes into the section from top to bottom (see Fig. 3c).

been reported in the literature (for a summary, see Robinson *et al.* 1982), but the sodic amphibole is typically glaucophane, not riebeckite.

Figure 4 graphically depicts the miscibility gap between sodic, calcic and Fe–Mg clinoamphiboles. In general, the gap is well defined, with only limited miscibility between the sodic-Fe–Mg and calcic-Fe–Mg end members. Sodic-calcic amphibole miscibility is variable. The largest gap is displayed by JCIF samples (triangles). This is due in part to our effort to avoid mixed compositions by analyzing the most sodic phase present, and in part to the probable low-temperature origin of this riebeckite.

CONTROLS ON AMPHIBOLE CHEMISTRY

The most notable compositional variation in coexisting amphiboles from the Jackson County Iron Formation is the $Fe^{2+}/(Fe^{2+} + Mg)$ ratio, which varies sympathetically with the amount of magnetite: as the amount of magnetite in the assemblage increases, the $Fe^{2+}/(Fe^{2+} + Mg)$ ratio in the amphibole decreases. This observation is also reported by Mueller (1960), Annersten (1968) and Floran & Papike (1978), and can be related to differences in $\mu(H_2O)$ and $\mu(O_2)$ between layers in the iron formation (discussed below). Other variations are also recorded, such as a positive correlation between the Al content of the amphibole and the $Fe^{2+}/(Fe^{2+} + Mg)$ ratio. These variations can largely be explained by the crystal chemistry and site preferences of the amphibole, as discussed below.

Cation site-preferences

The structural formula of the amphiboles can be represented as

A_1	$M4_2$	$M1_2$	$M3_1$	$M2_2$	T_8	O_{22}	$(OH)_2$
Na	Ca	Fe	Fe	Al	Si		OH^-
K	Na	Mg	Mg	Ti	Al		F^-
	Fe^{2+}			Fe^{3+}			Cl^-
	Mg			Mg			
	Mn			Fe^{2+}			

where the cation site-preferences are shown beneath each respective type of crystallographic site (*e.g.*, Hawthorne 1983). These cation site-preferences are important, as they can explain some of the compositional variations between coexisting amphiboles, such as different values of $Fe^{2+}/(Fe^{2+} + Mg)$. Similar rationale has been used by Robinson *et al.* (1982) to explain compositional relations in coexisting amphiboles.

For example, as mentioned previously, in the Al-poor amphibole pairs from the Jackson County Iron Formation, calcic amphibole (actinolite) has a lower $Fe^{2+}/(Fe^{2+} + Mg)$ than the coexisting Fe–Mg amphibole (cummingtonite) (Table 1). Considering the amphibole as being composed of 3 separate octahedral sites provides an explanation for this variation. Mössbauer data indicate that in Fe–Mg amphiboles, Fe^{2+} has a preference for the *M*4 site (Hawthorne 1983, Kimball 1981, Cameron & Papike 1979, Whittaker 1971, Burns & Prentice 1968, Bancroft *et al.* 1967). This preference is very pronounced in Mg-rich Fe–Mg amphiboles, such as cummingtonite, in which all Fe^{2+} present in the amphibole can be accommodated in *M*4 sites. Where the amount of Fe^{2+} in the amphibole exceeds the amount that will fit in *M*4 sites, the Fe^{2+} cations must occupy other sites, usually *M*1 and *M*3 in preference to *M*2 (Hawthorne 1983, Kimball 1981, Cameron & Papike 1979, Whittaker 1971, Burns & Prentice 1968, Bancroft *et al.* 1967).

Ca^{2+} will occupy the largest distorted octahedral site in the amphiboles, *M*4, which Fe^{2+} prefers. Consequently, amphiboles with a high calcium content tend to contain less Fe^{2+} than coexisting Fe–Mg amphiboles and have a lower value of $Fe^{2+}/(Fe^{2+} + Mg)$.

For the pair grunerite–hornblende, the $Fe^{2+}/(Fe^{2+} + Mg)$ is similar in both amphiboles. As in the nonaluminous assemblages the calcic amphibole (actinolite) has less Fe^{2+} than the coexisting Fe–Mg amphibole (grunerite). However, there is also less Mg^{2+} in the hornblende because Mg^{2+} is partitioned preferentially into the *M*2 site in amphiboles. But highly charged, small cations such as Al^{3+} are also partitioned preferentially into this site (Hawthorne 1983, Robinson *et al.* 1969, Cameron & Papike 1979). Consequently, Al^{3+} in the octahedral sites in hornblende is in the *M*2 sites, displacing Mg^{2+} from those sites.

$\mu(O_2)$–$\mu(H_2O)$ variations

The Fe-rich amphibole pair ferroactinolite–grunerite is found only in magnetite-poor sections

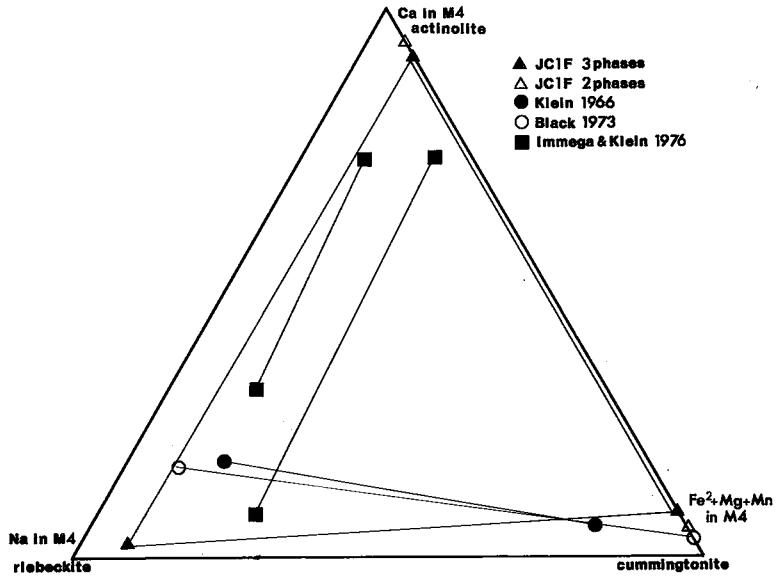

FIG. 4. Triangle plot of cation distribution in the *M*4 site of coexisting amphiboles. Plotted are two riebeckite–cummingtonite pairs from the literature (circles), a riebeckite–actinolite pair from the literature (squares), an actinolite–cummingtonite pair from the Jackson County Iron Formation (open triangles) and the three-phase assemblage riebeckite – actinolite – cummingtonite from the Jackson County Iron Formation (solid triangles).

of the iron formation, whereas actinolite–cummingtonite pairs occur in magnetite-rich samples. The differences between these assemblages cannot be explained in terms of variations in bulk composition, because the overall compositions are similar. But these differences in mineralogy are probably, at least in part, the results of local differences in the chemical potentials of oxygen $\mu(O_2)$ and water $\mu(H_2O)$. This can be explained qualitatively by considering that in areas of higher $\mu(O_2)$, more iron is oxidized, and much of the available iron is tied up in magnetite. Consequently, amphiboles and other silicates from magnetite-rich zones are relatively Fe-poor. In areas of low $\mu(O_2)$ most of the iron is incorporated into the amphiboles, making them Fe-rich.

This effect can be explained by the reaction

$$24SiO_2 + 7Fe_3O_4 + 3H_2O = 3Fe_7Si_8O_{22}(OH)_2 + \tfrac{7}{2}O_2 \quad (1)$$

which is a condition of heterogeneous equilibrium for the assemblage cummingtonite (or grunerite) + actinolite (or ferroactinolite) + quartz + magnetite. By inspection, it is apparent that an increase in $\mu(O_2)$ results in a decrease in the amount of grunerite component present in the amphibole, whereas an increase in $\mu(H_2O)$ results in an increase in the amount of that component.

Quantitative evaluation of the effect of $\mu(H_2O)$ and $\mu(O_2)$ on the phase relations can be made using Gibbs method (*e.g.*, Spear *et al.* 1982). To apply this type of analysis on the mineral assemblages in the iron formation requires a solution model for the Fe–Mg clinoamphiboles. The next section will describe briefly a two-site reciprocal solution model that we developed for this purpose.

Solution model for Fe–Mg amphibole. We have assumed that an Fe–Mg amphibole can be described in terms of two octahedral sites, the *M*4, which has a multiplicity of 2, and the "*M*123", which has a multiplicity of 5 (a combination of *M*1, *M*2 and *M*3 sites). Thus, we are considering Fe–Mg substitution over 2 distinct sites, which generates four different end-members:

X_1 $Mg_2Mg_5Si_8O_{22}(OH)_2$
X_2 $Fe_2Fe_5Si_8O_{22}(OH)_2$
X_3 $Fe_2Mg_5Si_8O_{22}(OH)_2$
X_4 $Mg_2Fe_5Si_8O_{22}(OH)_2$

only three of which are linearly independent. Choosing components 1, 2 and 3 to be independent, we can write the mole fractions of the three components as $X_1 = X_{Mg,M4}$, $X_2 = X_{Fe,M123}$, and $X_3 = X_{Mg,M123} - X_{Mg,M4}$, where the subscripts refer to the mole fractions of the cation on the indicated site.

Defining a reciprocal free-energy term

$$\Delta G^\circ_R = \mu^\circ_4 + \mu^\circ_3 - \mu^\circ_2 - \mu^\circ_1 \quad (2)$$

we can write (Wood & Nicholls 1978)

$$G_{SS} = X_{Mg,M4}\mu^\circ_1 + X_{Fe,M123}\mu^\circ_2 + (X_{Mg,M123} - X_{Mg,M4})\mu^\circ_3 + X_{Mg,M4}X_{Fe,M123}\Delta G^\circ_R + RT[X_{Mg,M4}\ell nX^2_{Mg,M4} + X_{Fe,M4}\ell nX^2_{Fe,M4}] + RT[X_{Mg,M123}\ell nX^5_{Mg,M123} + X_{Fe,M123}\ell nX^5_{Fe,M123}] \quad (3)$$

and

$$\mu_1 = \mu^\circ_1 + X_{Fe,M123}X_{Fe,M4}\Delta G^\circ_R + RT(\ell nX^2_{Mg,M4} + \ell nX^5_{Mg,M123}) \quad (4)$$

$$\mu_2 = \mu^\circ_2 + X_{Mg,M123}X_{Mg,M4}\Delta G^\circ_R + RT(\ell nX^2_{Fe,M4} + \ell nX^5_{Fe,M123}) \quad (5)$$

$$\mu_3 = \mu^\circ_3 + X_{Fe,M123}X_{Mg,M4}\Delta G^\circ_R + RT(\ell nX^2_{Fe,M4} + \ell nX^5_{Mg,M123}) \quad (6)$$

Evaluation of ΔG°_R. To our knowledge there are no published values for reciprocal ΔG in amphiboles in the literature. However, an estimate can be obtained using the compositions of coexisting Fe–Mg and Ca-amphiboles. Consider the Fe–Mg exchange:

$$\underset{(FM)}{Fe_2Fe_5Si_8O_{22}(OH)_2} + \underset{(CA)}{Ca_2Mg_5Si_8O_{22}(OH)_2} = \underset{(FM)}{Fe_2Mg_5Si_8O_{22}(OH)_2} + \underset{(CA)}{Ca_2Fe_5Si_8O_{22}(OH)_2} \quad (7)$$

We can write an equation among the chemical potentials of these components, and this equation can be expanded to

$$0 = \Delta\mu^\circ + 5RT\ell nK - X_{Mg,M4}\,\Delta G^\circ_R \quad (8)$$

where $$K = \left[\frac{X_{Fe}}{X_{Mg}}\right]_{CA} \bullet \left[\frac{X_{Mg,M123}}{X_{Fe,M123}}\right]_{FM} \quad (9)$$

and CA and FM represent the calcic and Fe–Mg amphiboles, respectively. Site occupancies in the Fe–Mg amphibole were calculated from the constraints

$$Fe,M123 + Mg,M123 = 5 \quad (10a)$$

$$Fe,M4 + Mg,M4 = 2 \quad (10b)$$

$$Fe,M123 + Fe,M4 = Fe,Total \quad (10c)$$

and

$$K_{123,4} = \frac{(Fe,M123)}{(Mg,M123)} \bullet \frac{(Mg,M4)}{(Fe,M4)} = 0.1 \quad (10d)$$

The value of 0.1 for $K_{123,4}$, the intracrystalline Fe-Mg distribution coefficient, was chosen as an average value from that obtained on heat-treated cummingtonite by Ghose & Weidner (1971, 1972; *i.e.*, between 0.08 amd 0.13 at 550°C). The effect of this choice of $K_{123,4}$ on the calculated results will be discussed later.

From equation (9) it can be seen that a plot of ℓnK *versus* $X_{Mg,M4}$ would have a slope of $\Delta G^\circ_R/5RT$ and an intercept of $-\Delta\mu^\circ/5RT$. Utilizing all data on coexisting actinolite and cummingtonite from the Jackson County Iron Formation, such a plot reveals that ΔG°_R is approximately 0, with an estimated error of ± 6 kcal. The effect of this uncertainty of ΔG°_R on our results will be discussed later.

Gibbs method. The Gibbs method (*e.g.*, Spear *et al.* 1982) is a technique whereby changes in mineral composition can be used as monitors of changes in other intensive parameters, in this case $\mu(O_2)$ and $\mu(H_2O)$. The procedure involves first an analytical formulation of the phase equilibria of the rock, and then solving the system of equations for the desired derivatives. In this case we wish to examine how $\mu(O_2)$ and $\mu(H_2O)$ change with X_{Fe} in cummingtonite, so we will use $X_{Fe,M123}$ $(= X_2)$ as the monitor and solve for the derivatives $[\delta\mu(O_2)/\delta X_2]_{P,T,\mu(H_2O)}$, $[\delta\mu(H_2O)/\delta X_2]_{P,T,\mu(O_2)}$ and $[\delta\mu(O_2)/\delta\mu(H_2O)]_{P,T,X_2}$. The value $X_{Fe,bulk}$ can always be recovered through equations 10.

The necessary equations to formulate analytically the phase equilibria are one Gibbs-Duhem equation for each phase, a set of linearly independent conditions of heterogeneous equilibria among the phase components of minerals in the assemblage, and equations to introduce the variable dX_2. For the assemblage Fe-Mg-amphibole + Ca-amphibole + magnetite + quartz, this yields 4 Gibbs-Duhem equations, three conditions of heterogeneous equilibrium, equations (1) and (7) and the following equation:

$$5Mg_7Si_8O_{22}(OH)_2 + 7Ca_2Fe_5Si_8O_{22}(OH)_2 = 5Fe_7Si_8O_{22}(OH)_2 + 7Ca_2Mg_5Si_8O_{22}(OH)_2 \qquad (11)$$

Because we would like to describe variations in $\mu(O_2)$ and $\mu(H_2O)$ as a function of amphibole com-

TABLE 3. SYSTEM OF HOMOGENEOUS EQUATIONS IN MATRIX FORM FOR THE MULTIVARIANT EQUILIBRIUM Fe-Mg AMPHIBOLE + Ca-AMPHIBOLE + QUARTZ + MAGNETITE

$$\begin{bmatrix}
\bar{S}^{FM} & -\bar{V}^{FM} & X_1^{FM} & X_2^{FM} & X_3^{FM} & 0 & 0 & 0 & 0 & 0 & 0 & 0 & 0 \\
\bar{S}^{CA} & -\bar{V}^{CA} & 0 & 0 & 0 & X_{Fe}^{CA} & X_{Mg}^{CA} & 0 & 0 & 0 & 0 & 0 & 0 \\
\bar{S}^{Q} & -\bar{V}^{Q} & 0 & 0 & 0 & 0 & 0 & 1 & 0 & 0 & 0 & 0 & 0 \\
\bar{S}^{M} & -\bar{V}^{M} & 0 & 0 & 0 & 0 & 0 & 0 & 1 & 0 & 0 & 0 & 0 \\
0 & 0 & 5 & -5 & 0 & 7 & -7 & 0 & 0 & 0 & 0 & 0 & 0 \\
0 & 0 & 0 & -3 & 0 & 0 & 0 & 24 & 7 & 3 & -7/2 & 0 & 0 \\
0 & 0 & 0 & -1 & 1 & 1 & -1 & 0 & 0 & 0 & 0 & 0 & 0 \\
-(\bar{S}_1^{FM} - \bar{S}_3^{FM}) & (\bar{V}_1^{FM} - \bar{V}_3^{FM}) & -1 & 0 & 1 & 0 & 0 & 0 & 0 & 0 & 0 & G^{11} & G^{12} \\
-(\bar{S}_2^{FM} - \bar{S}_3^{FM}) & (\bar{V}_2^{FM} - \bar{V}_3^{FM}) & 0 & -1 & 1 & 0 & 0 & 0 & 0 & 0 & 0 & G^{12} & G^{22}
\end{bmatrix}
\begin{bmatrix} dT \\ dP \\ d\mu(FM_1) \\ d\mu(FM_2) \\ d\mu(FM_3) \\ d\mu(CA_{Fe}) \\ d\mu(CA_{Mg}) \\ d\mu(Q) \\ d\mu(M) \\ d\mu(H_2O) \\ d\mu(O_2) \\ dX_1^{FM} \\ dX_2^{FM} \end{bmatrix}
=
\begin{bmatrix} 0 \\ 0 \\ 0 \\ 0 \\ 0 \\ 0 \\ 0 \\ 0 \\ 0 \\ 0 \\ 0 \\ 0 \\ 0 \end{bmatrix}$$

Symbols:

FM Fe-Mg amphibole, CA calcic amphibole, Q quartz, M magnetite, Fe Fe-end member, Mg Mg-end member, 1 $Mg_2Mg_5Si_8O_{22}(OH)_2$, 2 $Fe_2Fe_5Si_8O_{22}(OH)_2$ 3 $Fe_2Mg_5Si_8O_{22}(OH)_2$. G^{11}, G^{12} and G^{22} as defined in text.

position, it is necessary to introduce the variables dX_1^{FM}, and dX_2^{FM}. This can be done with equations that are the complete differentials of $(\mu_1^{FM}-\mu_3^{FM})$ $(\mu_2^{FM}-\mu_3^{FM})$ in the Fe–Mg amphibole:

$$d(\mu_1^{FM}-\mu_3^{FM}) = -(\bar{S}_1^{FM}-\bar{S}_3^{FM})dT+(\bar{V}_1^{FM}-\bar{V}_3^{FM})dP+\left[\frac{\delta^2 G_{SS}^{FM}}{\delta X_1 \delta X_2}\right]_{P,T} dX_2^{FM}+\left[\frac{\delta^2 G_{SS}^{FM}}{\delta X_1^2}\right]_{P,T} dX_1^{FM} \quad (12)$$

$$d(\mu_2^{FM}-\mu_3^{FM}) = -(\bar{S}_2^{FM}-\bar{S}_3^{FM})dT+(\bar{V}_2^{FM}-\bar{V}_3^{FM})dP+\left[\frac{\delta^2 G_{SS}^{FM}}{\delta X_2^2}\right]_{P,T} dX_2^{FM}+\left[\frac{\delta^2 G_{SS}^{FM}}{\delta X_1 \delta X_2}\right]_{P,T} dX_1^{FM} \quad (13)$$

Equations 1, 7, and 11 written in terms of the differentials of chemical potentials, plus equations 12 and 13 and four Gibbs–Duhem equations (one for each phase present) can be written as a matrix of 9 linear equations in the 13 unknowns: dT, dP, dX_1^{FM}, dX_2^{FM}, $d\mu(O_2)$, $d\mu(H_2O)$, $d\mu$(quartz), $d\mu$(magnetite), $d\mu(FM_1)$, $d\mu(FM_2)$, $d\mu(FM_3)$, $d\mu(CA)_{Mg}$ and $d\mu(CA)_{Fe}$ (Table 3). The Ca-amphibole (CA) is assumed to be a binary Fe–Mg solution on the $M123$ site.

If pressure and temperature are assumed to be constant over the sample area and one other variable is held constant [*e.g.*, $d\mu(H_2O)$ or $d\mu(O_2)$], then it is possible to obtain solutions for *ratios* of any two of these variables.

For example,

$$\left[\frac{\delta\mu(O_2)}{\delta X_2}\right]_{P,T,\mu(H_2O)} = \frac{(-15X_3-21X_1)(G^{12}G^{12}-G^{11}G^{22})}{-7/2(5G^{11}+2G^{12})} \quad (14)$$

$$\left[\frac{\delta\mu(H_2O)}{\delta X_2}\right]_{P,T,\mu(O_2)} = \frac{(-15X_3-21X_1)(G^{12}G^{12}-G^{11}G^{22})}{3(5G^{11}+2G^{12})} \quad (15)$$

and

$$\left[\frac{\delta\mu(O_2)}{\delta\mu(H_2O)}\right]_{P,T,X_2^{FM}} = \frac{6}{7} \quad (16)$$

where

$$G^{11} = \left[\frac{\delta^2 G_{SS}^{FM}}{\delta X_1^2}\right]_{P,T}$$

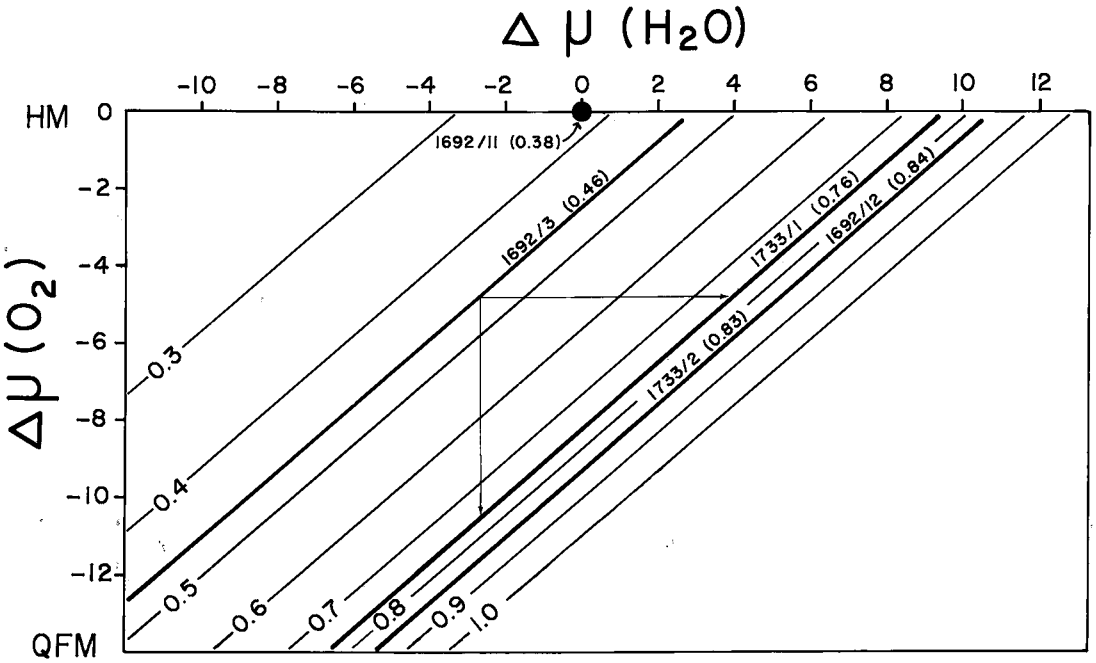

FIG. 5. $\Delta\mu(O_2)$ – $\Delta\mu(H_2O)$ diagram contoured with $X_{Fe,bulk}^{FM}$. The origin (0,0) is arbitrarily chosen at $X_{Fe,bulk}^{FM}$ = 0.38 (sample 1692/11) at a $\mu(O_2)$ equivalent to the hematite – magnetite (HM) buffer. Lower limit of $\mu(O_2)$ is taken at the quartz–fayalite–magnetite buffer (QFM) buffer. Values of $\Delta\mu(H_2O)$ and $\Delta\mu(O_2)$ are given in kcal. Thin lines are contours of 0.1 $X_{Fe,bulk}^{FM}$ intervals. Thick lines are samples locations in μ–μ space. Arrows show possible differences in fluid composition from samples 1692/3 to 1733/1.

$$G^{12} = \left[\frac{\delta^2 G_{SS}^{FM}}{\delta X_1 \delta X_2}\right]_{P,T}$$

$$G^{22} = \left[\frac{\delta^2 G_{SS}^{FM}}{\delta X_2^2}\right]_{P,T}$$

Using equation 3 to define G_{SS}^{FM} and taking the appropriate derivatives

$$G^{11} = \frac{2RT}{X_{Mg,M4} \cdot X_{Fe,M4}}$$

$$G^{12} = \Delta G_R^\circ$$

$$G^{22} = \frac{5RT}{X_{Mg,M123} \cdot X_{Fe,M123}}$$

A $\mu(O_2)$–$\mu(H_2O)$ diagram has been drawn contoured relative to $X_{Fe,\,bulk}^{FM}$ by numerical integration of equations 14 and 15 (Fig. 5). This integration provides only relative changes of $\mu(O_2)$ and $\mu(H_2O)$; to construct the diagram it is necessary to choose an arbitrary reference-point where $\Delta\mu(O_2) = \Delta\mu(H_2O) = 0$. The reference point was chosen to be sample 1692/11, which contains the assemblage cummingtonite + quartz + magnetite + hematite with $X_{Fe}^{FM} = 0.38$. Thus, $\Delta\mu(O_2)$ will be evaluated relative to the hematite–magnetite buffer curve. There are no assemblages of quartz + fayalite + magnetite; consequently the QFM buffer can be considered the lower limit of $\mu(O_2)$ in the iron formation [$\Delta\mu(O_2) \approx -14$ kcal]. The resulting diagram (Fig. 5) quantitatively shows the effect of $\mu(O_2)$ and $\mu(H_2O)$ on the composition of the amphibole. At constant P and T, increasing $\mu(O_2)$ at constant $\mu(H_2O)$ results in decreasing Fe contents, whereas increasing $\mu(H_2O)$ at constant P,T and $\mu(O_2)$ results in increasing Fe contents. To maintain constant composition, both variables must be increased or decreased simultaneously. If two assemblages contain amphibole + magnetite + hematite [$\mu(O_2)$ is at the magnetite–hematite buffer], the grunerite with the highest (X_{Fe}^{FM}) formed at the highest value of μH_2O. Because the lines of constant composition (X_{Fe}^{FM}) are closer together at higher X_{Fe}^{FM}, the changes in $\mu(H_2O)$ and $\mu(O_2)$ indicated by changing composition of the amphibole are smaller in the more Fe-rich Fe–Mg amphiboles.

Using equations 14 and 15 (or Fig. 5) with the amphibole compositions in Table 1 and the distances between samples, gradients in $\mu(O_2)$ and $\mu(H_2O)$ within the iron formation can be computed. However, because there are two independent parameters, $\mu(O_2$ and $\mu(H_2O)$, it is not possible to compute a gradient in one without fixing the other. This has been done, and values of $\Delta\mu(O_2)$ at constant P, T and $\mu(H_2O)$, and of $\Delta\mu(H_2O)$ at constant P,T and $\mu(O_2)$ are presented in Table 4. Actual gradients, if $\mu(O_2)$ and $\mu(H_2O)$ vary sympathetically, will be different from the tabulated values, but these numbers give an approximate range of expected gradients recorded by different assemblages in the iron formation. The effect of the assumptions regarding the solid-solution model for cummingtonite on the values shown in Table 4 are as follows. The values in Table 4 were computed assuming a two-site solution model with a value $K_{123,4} = 0.1$ and $\Delta G_R^\circ = 0$. Choosing $K_{123,4} = 1.0$ (*i.e.*, a one-site model) or $K_{123,4} = 0.01$ changes the listed values by $\mp 13\%$. Choosing $K_{123,4} = 0.1$ and $\Delta G_R^\circ = \pm 10$ kcal changes the listed values by -16% and $+2\%$, respectively. For example, for the first listed oxygen gradient in Table 4 (1692/3–1692/12), the total range of computed values considering all possible assumptions is 36–49 cal/metre compared with 43 cal/metre using our preferred values of $K_{123,4} = 0.1$ and $\Delta G_R^\circ = 0$. Therefore, it can be concluded that the choice of solution model has only a minor effect on the results.

TABLE 4. GRADIENTS IN $\mu(O_2)$ AND $\mu(H_2O)$ BETWEEN IRON FORMATION SAMPLES

Sample 1–Sample 2*	distance (meters)	$\Delta\mu(O_2)$ cal/m	$\Delta\mu(H_2O)$ cal/m
1692/3 – 1692/12	157	43	-50
1692/3 – 1733/1	109	65	-76
1692/3 – 1733/2	260	25	-30
1692/12 – 1733/2	145	-1	1
1692/12 – 1733/1	191	2	-2
1733/2 – 1733/1	515	1	-1

* $\Delta\mu(O_2)$ and $\Delta\mu(H_2O)$ are calculated as $\mu(O_2)$ in sample 1 – $\mu(O_2)$ in sample 2 etc.

As can be seen from Table 4, gradients range from a few calories/metre to approximately 75 cal/m. In Figure 6, maximum gradients in the chemical potential of H_2O, as determined from studies on quartzite, amphibolite, pelite and calc-silicate, are shown. The maximum calculated gradients in $\mu(H_2O)$ in the iron formation is similar to that in quartzite, which is interesting considering that the dominant matrix-mineral in the iron formation is quartz. It may be that these gradients are reflecting the relative permeability of different rock-types under metamorphic conditions.

The significance of the gradients plotted in Figure 6 deserve some discussion. These gradients are calculated by dividing the value of $\Delta\mu(H_2O)$ recorded by two assemblages by the distance between the two samples. As such, they really represent *minimum* gradients, because the nature of $\Delta\mu(H_2O)$ between the two samples is not known [for example, the $\mu(H_2O)$ gradient may actually be very steep over a short distance, instead of gradual as assumed in this calcula-

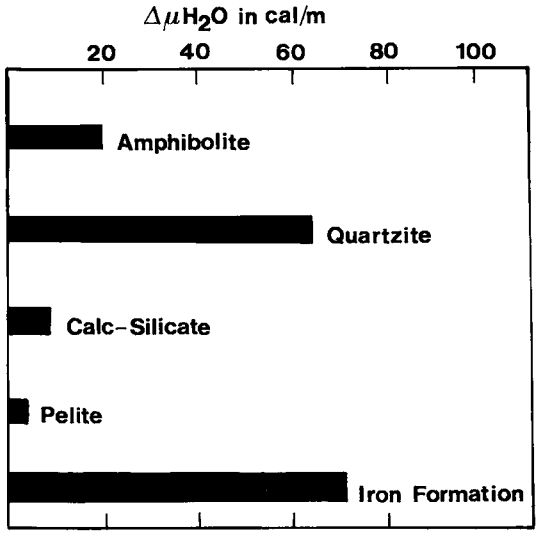

FIG. 6. Chemical potential gradients for H_2O in cal/m in various rock types: amphibolite (Spear 1977), quartzite (Rumble 1978), calc-silicate (Ferry 1979), pelite (Grambling 1981) and iron formation (this study). Taken in part from Spear *et al.* (1982).

tion]. It would be informative to know the magnitude of chemical potential gradients that can be sustained by different rock-types undergoing regional metamorphism, because this would provide knowledge of element mobility during the metamorphic process. This would require a detailed study on the scale of a thin section, across compositional layers that record different values of $\mu(H_2O)$.

One conclusion that can be drawn from Figures 5 and 6 is that individual layers record different values of the chemical potentials of H_2O or O_2 (or both) and that these values were preserved during metamorphism. As suggested by Rumble (1978) for the Clough Quartzite on Black Mountain, New Hampshire, the different water and oxygen contents were probably inherited from the original sedimentary environment. Preservation during metamorphism is a function of the buffering capacity of the mineral assemblage and the rate of fluid infiltration, as discussed by Spear *et al.* (1982).

DISCUSSION

The Jackson County Iron Formation displays several interesting features: the talc schist core, the presence of altered volcanic rocks in the periphery, the riebeckite–cummingtonite intergrowths, and the marked gradients in chemical potential of O_2 and H_2O. Moreover, this deposit is most likely volcanogenic, formed in an oceanic (*e.g.*, seawater) environment (see below). Any model for the origin of this deposit must take these features into account.

Talc schist

The talc schist zone at the mine most probably represents an alteration pipe related to a hydrothermal vent on the sea floor (Jones 1978). This seems reasonable as alteration zones associated with volcanic-exhalative ore deposits are characteristically Mg-rich. For example, the alteration pipe at the Mattagami Lake mine, Quebec, grades, within 3 metres, from a chlorite-rich tuff to talc–chlorite schist to talc schist or talc–actinolite schist (Roberts & Reardon 1978). This alteration pipe is assumed to have been the discharge site of a thermally induced system of convective flow. The gradation from pure talc in the centre of the zone to the more aluminous talc–chlorite asssemblage at the edge is considered to have been caused by a higher flux of seawater in the centre (Roberts & Reardon 1978). The talc at the centre of the pipe may also represent alteration at lower temperature, higher SiO_2 activity or higher water/rock ratios than the chlorite-bearing assemblages at the edge of the zone. Definitive statements about the nature of the talc schist are difficult because deformation of the rocks obscures the original shape of the talc schist zone. In fact, it is not certain whether the talc schist is above or below the iron formation. If the talc zone is an alteration pipe, then the amphibolite layers concordant with the iron formation may be metamorphosed tuff units or hydrothermally altered volcanic units with a lower water/rock ratio.

Riebeckite

The riebeckite–cummingtonite intergrowths have been found only in magnetite-rich samples from the iron formation. This suggests a correlation of riebeckite formation with high fugacity of oxygen. The riebeckite-core texture indicates that the riebeckite is probably a precursor to the cummingtonite. The association of riebeckite with cracks in the host cummingtonite is interpreted as a result of late-stage alteration of cummingtonite by Na-rich fluids.

Massive riebeckite-bearing beds in low-grade iron formation have been reported from Australia (Klein & Gole 1981, Gole 1980, Grubb 1971, Trendall 1973, Smith *et al.* 1982) and South Africa (Beukes 1973). It is possible that the riebeckite-bearing layer in the Jackson County Iron Formation was originally a massive bed of riebeckite such as these, but the paucity of riebeckite-bearing samples implies that the sedimentary iron-formation contained only a few dispersed layers of riebeckite.

Origin of the iron formation

A possible scenario for the origin of the iron formation assumes the protolith to be a Si–, Fe–rich gel

formed in an environment of shallow seawater (*e.g.*, Bayley & James 1973, Beukes 1973, Drever 1974, Kranck 1961). The original sediment may be continentally derived, or volcanic, or a mixture of the two. The talc schist zone at the Jackson County mine suggests that the sediments were, at least in part, volcanogenic. In this case, the Na-rich layer necessary for riebeckite formation probably represents an evaporite bed within this sequence (Gole 1980, Milton *et al.* 1974, Miyano & Klein 1983).

Progressive metamorphism of this sedimentary pile would evolve riebeckite in the Na-rich evaporite bed (after reactions such as those described in Miyano & Klein 1983) and magnetite, carbonate, minnesotaite, stilpnomelane and chlorite in the rest of the iron formation (*e.g.*, Klein 1973, 1974, 1978, Haase 1982, Floran & Papike 1978, Kranck 1961). Further progressive metamorphism results in the formation of amphiboles (Klein 1973, 1978, Haase 1982, Floran & Papike 1978, Kranck 1961, Frost 1979, Immega & Klein 1976) and eventually, pyroxene (Haase 1982, Immega & Klein 1976, Dimroth & Chauvel 1973, Bonnichsen 1969, Butler 1969) For example, reactions producing cummingtonite from riebeckite may be driven by acid metasomatism: $2Na_2Fe^{2+}{}_3Fe^{3+}{}_2Si_8O_{22}(OH)_2 + 4HCl = Fe_7Si_8O_{22}(OH)_2 + 4NaCl + 1/2O_2 + 3H_2O + Fe_3O_4 + 8SiO_2$. This reaction also produces an NaCl brine along with magnetite (or hematite) and quartz. Halite daughter crystals have been found in fluid inclusions in quartz in the iron formations, supporting this reaction mechanism.

The marked gradients in chemical potential recorded by the mineral assemblages in the iron formation must have been inherited from the original heterogeneity of the sedimentary sequence. This is also consistent with an original deposition of the protolith in a closed basin, with different layers incorporating different quantities of reduced *versus* oxidized *versus* hydrated assemblages. Preservation of these original sedimentary heterogeneities implies that metamorphism was accompanied by a limited amount of infiltration, such that the buffering capacity of the mineral assemblages was not exceeded. Finally, riebeckite alteration along cracks within cummingtonite suggests that Na-rich fluids were remobilized late in the metamorphic evolution of these rocks.

Acknowledgements

The Inland Steel Company graciously allowed numerous visits to the Jackson County iron mine and provided drill core and mine maps. Much of this work was done at the University of Wisconsin, while Kimball was a graduate student. That part of the research was supported largely by a National Science Foundation grant to C.V. Guidotti (EAR-7902597). The field work was supported by a grant from the Exxon Company. Most of the electron microprobe analyses were made on the ARL microprobe at the University of Chicago. Support for the work completed at MIT was from a National Science Foundation Grant to F.S. Spear (EAR81-08617). C.V. Guidotti was particularly supportive and encouraging during all phases of this research. Discussions with E.N. Cameron, C. Klein, W.C. Shanks, D.G. Jones, R. Maas, C.S. Haase, R.A. Zierenberg and G. Jilson were helpful. Reviews of this manuscript by L.G. Woodruff and the anonymous referees are greatly appreciated.

References

Annersten, H. (1968): A mineral chemical study of a metamorphosed iron formation on northern Sweden. *Lithos* **1**, 374-397.

Bancroft, G.M., Maddock, A.G. & Burns, R.G. (1967): Applications of the Mössbauer effect to silicate mineralogy. I. Iron silicates of known crystal structure. *Geochim. Cosmochim. Acta* **31**, 2219-2246.

Bayley, R.W. & James, H.L. (1973): Precambrian iron-formations of the United States. *Econ. Geol.* **68**, 934-959.

Beukes, N.J. (1973): Precambrian iron-formations of southern Africa. *Econ. Geol.* **68**, 960-1004.

Black, P.M. (1973): Mineralogy of New Caledonian metamorphic rocks. II. Amphiboles from the Ouégoa district. *Contr. Mineral. Petrology* **39**, 55-64.

Bonnichsen, B. (1969): Metamorphic pyroxenes and amphiboles in the Biwabik Iron Formation, Dunka River area, Minnesota. *Mineral. Soc. Amer. Spec. Pap.* **2**, 217-239.

Burns, R.G. & Prentice, F.J. (1968): Distribution of iron cations in the crocidolite structure. *Amer. Mineral.* **53**, 770-776.

Butler, P., Jr. (1969): Mineral compositions and equilibria in the metamorphosed iron formation of the Gagnon region, Quebec, Canada. *J. Petrology* **10**, 56-101.

Cameron, M. & Papike, J.J. (1979): Amphibole crystal chemistry: a review. *Fortschr. Mineral.* **57**, 28-67.

Dimroth, E. & Chauvel, J.-J. (1973): Petrography of the Sokoman Iron Formation in part of the central Labrador Trough, Quebec, Canada. *Geol. Soc. Amer. Bull.* **84**, 111-134.

Drever, J.I. (1974): Geochemical model for the origin of Precambrian banded iron formations. *Geol. Soc. Amer. Bull.* **85**, 1099-1106.

ESKOLA, P. (1915): On the relations between the chemical and mineralogical composition in the metamorphic rocks of the Orijarvi region. *Comm. Géol. Finlande Bull.* **44,** 109-145.

FERRY, J.M. (1979): A map of chemical potential differences within an outcrop. *Amer. Mineral.* **64,** 966-985.

FLORAN, R.J. & PAPIKE, J.J. (1978): Mineralogy and petrology of the Gunflint iron formation, Minnesota-Ontario: correlation of compositional and assemblage variations at low to moderate grade. *J. Petrology* **19,** 215-288.

FROST, B.R. (1979): Metamorphism of iron-formation: parageneses in the system Fe–Si–C–O–H. *Econ. Geol.* **74,** 774-785.

GHOSE, S. & WEIDNER, J.R. (1971): Mg^{2+}–Fe^{2+} distribution isotherms in cummingtonites at 600°C and 700°C. *Amer. Geophys. Union Trans.* **52,** 381 (abstr.).

_____ & _____ (1972): Mg^{2+}–Fe^{2+} order–disorder in cummingtonite, $(Mg,Fe)_7Si_8O_{22}(OH)_2$: a new geothermometer. *Earth Planet. Sci. Lett.* **16,** 346-354.

GOLE, M.J. (1980): Low-temperature retrograde minerals in metamorphosed Archean banded iron-formations, Western Australia. *Can. Mineral.* **18,** 205-214.

GRAMBLING, J.A. (1981): Kyanite, andalusite, sillimanite, and related mineral assemblages in the Truchas Peaks region, New Mexico. *Amer. Mineral.* **66,** 702-722.

GRUBB, P.L.C. (1971): Silicates and their paragenesis in the Brockman Iron Formation of Wittenoom Gorge, Western Australia. *Econ. Geol.* **66,** 281-292.

HAASE, C.S. (1982): Metamorphic petrology of the Negaunee Iron Formation, Marquette District, northern Michigan: mineralogy, metamorphic reactions, and phase equilibria. *Econ. Geol.* **77,** 60-81.

HAWTHORNE, F.C. (1983): The crystal chemistry of the amphiboles. *Can. Mineral.* **21,** 173-480.

IMMEGA, I. P. & KLEIN, C., JR. (1976): Mineralogy and petrology of some metamorphic Precambrian iron-formations in southwestern Montana. *Amer. Mineral.* **61,** 1117-1144.

JONES, D.G. (1978): *Geology of the Iron Formation and Associated Rocks of the Jackson County Iron Mine, Jackson County, Wisconsin.* M.S. thesis, Univ. Wisconsin, Madison, Wisc.

KIMBALL, K.L. (1981): *Phase Relations in Coexisting Fe–Mg and Ca Amphiboles.* Ph.D. thesis, Univ. Wisconsin, Madison, Wisc.

KLEIN, C., JR. (1966): Mineralogy and petrology of the metamorphosed Wabush iron formation, southwestern Labrador. *J. Petrology* **7,** 246-305.

_____ (1968): Coexisting amphiboles. *J. Petrology* **9,** 281-330.

_____ (1973): Changes in mineral assemblages with metamorphism of some banded Precambrian iron-formations. *Econ. Geol.* **68,** 1075-1088.

_____ (1974): Greenalite, stilpnomelane, minnesotaite, crocidolite and carbonates in a very low-grade metamorphic Precambrian iron-formation. *Can. Mineral.* **12,** 475-498.

_____ (1978): Regional metamorphism of Proterozoic iron-formation, Labrador Trough, Canada. *Amer. Mineral.* **63,** 898-912.

_____ & GOLE, M.J. (1981): Mineralogy and petrology of parts of the Marra Mamba Iron Formation, Hamersley Basin, Western Australia. *Amer. Mineral.* **66,** 507-525.

KRANCK, S.H. (1961): A study of phase equilibria in a metamorphic iron formation. *J. Petrology* **2,** 137-184.

LAIRD, J. & ALBEE, A.L. (1981): Pressure, temperature, and time indicators in mafic schist: their application to reconstructing the polymetamorphic history of Vermont. *Amer. J. Sci.* **281,** 127-175.

LEAKE, B.E. (1978): Nomenclature of amphiboles. *Can. Mineral.* **16,** 501-520.

MILTON, C., INGRAM, B. & BREGER, I. (1974): Authigenic magnesioarfvedsonite from the Green River Formation, Duchesne County, Utah. *Amer. Mineral.* **59,** 830-836.

MIYANO, T. & KLEIN, C. (1983): Conditions of riebeckite formation in the iron-formation of the Dales Gorge Member, Hamersley Group, Western Australia. *Amer. Mineral.* **68,** 517-529.

MUELLER, R.F. (1960): Compositional characteristics and equilibrium relations in mineral assemblages of a metamorphosed iron formation. *Amer. J. Sci.* **258,** 449-497.

ROBERTS, R.G. & REARDON, E.J. (1978): Alteration and ore-forming processes at Mattagami Lake Mine, Quebec. *Can. J. Earth Sci.* **15,** 1-21.

ROBINSON, P., JAFFE, H.W., KLEIN, C., JR. & ROSS, M. (1969): Equilibrium coexistence of three amphiboles. *Contr. Mineral. Petrology* **22,** 248-258.

_____, SPEAR, F.S., SCHUMACHER, J.C., LAIRD, J., KLEIN, C., EVANS, B.W. & DOOLAN, B.L. (1982): Phase relations of metamorphic amphiboles: natural occurrence and theory. *In* Amphiboles: Petrology and Experimental Phase Relations (D.R. Veblen & P.H. Ribbe, eds.). *Mineral. Soc. Amer., Rev. Mineral.* **9B,** 1-227.

RUMBLE, D., III (1978): Mineralogy, petrology, and oxygen isotopic geochemistry of the Clough Formation, Black Mountain, western New Hampshire, U.S.A. *J. Petrology* **19,** 317-340.

SMITH, R.E., PERDRIX, J.L. & PARKS, T.C. (1982): Burial metamorphism in the Hamersley Basin, Western Australia. *J. Petrology* **23,** 75-102.

SPEAR, F.S. (1977): Phase equilibria of amphibolites from the Post Pond Volcanics, Vermont. *Carnegie Inst. Wash. Year Book* **76,** 613-619.

_____, FERRY, J.M. & RUMBLE, D., III (1982): Analytical formulation of phase equilibria: the Gibbs method. *In* Characterization of Metamorphism Through Mineral Equilibria (J.M. Ferry, ed.). *Mineral. Soc. Amer., Rev. Mineral.* **10,** 105-152.

_____ & KIMBALL, K.L. (1983): RECAMP – a Fortran IV program for estimating Fe^{3+} contents in amphiboles. *Comp. Geosci.* (in press).

TRENDALL, A.F. (1973): Precambrian iron-formations of Australia. *Econ. Geol.* **68,** 1023-1034.

WHITTAKER, E.J.W. (1971): Madelung energies and site-preferences in amphiboles I. *Amer. Mineral.* **56,** 980-996.

WOOD, B.J. & NICHOLLS, J. (1978): The thermodynamic properties of reciprocal solid solutions. *Contr. Mineral. Petrology* **66,** 389-400.

Received July 14, 1983, revised manuscript accepted February 23, 1984.